Controlled Light-Matter Coupling for a Single Quantum Dot Embedded in a Pillar Microcavity Using Far-Field Optical Lithography

A. Dousse, L. Lanco,* J. Suffczyński, E. Semenova, A. Miard, A. Lemaître, I. Sagnes, C. Roblin, J. Bloch, and P. Senellart†

Laboratoire de Photonique et Nanostructures, LPN/CNRS, Route de Nozay, 91460 Marcoussis, France

(Received 4 July 2008; published 31 December 2008)

Using far-field optical lithography, a single quantum dot is positioned within a pillar microcavity with a 50 nm accuracy. The lithography is performed *in situ* at 10 K while measuring the quantum dot emission. Deterministic spectral and spatial matching of the cavity-dot system is achieved in a single step process and evidenced by the observation of strong Purcell effect. Deterministic coupling of two quantum dots to the same optical mode is achieved, a milestone for quantum computing.

DOI: 10.1103/PhysRevLett.101.267404 PACS numbers: 78.55.Cr, 42.50.Pq, 78.67.Hc, 81.16.Nd

Quantum emitters such as quantum dots [1], colloidal quantum dots [2], or a single fluorescent molecule [3] are usually randomly distributed on the surface of a substrate and suffer from broad inhomogeneous distributions of their spectral lines. Although spectral identification and spatial localization of individual quantum emitters is made possible using high resolution confocal microspectroscopy, the fabrication of devices involving dots of known position and spectral characteristics remains a serious experimental challenge.

An example of such a device is a quantum dot (QD) whose emission and location are matched to an optical microcavity mode. Such devices are desirable for high throughput and directional single photon sources [4–7] and for building blocks for quantum computing [8–11]. A deterministic and scalable fabrication method allowing choosing a single QD of given spectral characteristics to be inserted in an optical device with an accuracy of few tens of nanometers is missing. This is a prohibiting barrier to the development of solid state quantum emitter devices as well as to comprehensive fundamental investigations of solid state cavity quantum electrodynamics (CQED).

Earlier CQED investigations with single QDs or nanocrystals were based on statistical approaches by which several thousands of devices were fabricated [12–16]. It was left to pure statistics and prohibitively long searches to get the appropriate QD at the appropriate location of the cavity as the yield was in the low 10^{-3}. Lately, the need for control of the QD-cavity matching has motivated many works [17–22]. In a pioneer work, Badolato and co-workers successfully demonstrated deterministic cavity-QD coupling [23]. The spatial positioning of the QD was achieved using several technological steps (AFM, electronic lithography) each requiring an alignment accuracy of the order of 10 nm. The spectral matching was obtained thanks to several wet-etching steps, preventing the fabrication of more than one cavity-QD device on a given sample.

In this Letter, we show that a far-field optical lithography can be used to position a single QD in a spectrally resonant pillar microcavity with an accuracy as high as 50 nm. The lithography is performed *in situ*, while measuring the QD emission in a low-temperature photoluminescence setup. The nanopositioning is obtained by using the single QD as a probe of a focused Gaussian laser beam. The cavity-QD spectral matching is achieved in the same lithography step by selecting a QD of given spectral position and making use of the nonlinearity of the resist exposure process. The efficiency of the technique is shown by the observation of large controlled Purcell effect. The flexibility of our technique allows us to deterministically couple, for the first time, two QDs to the same optical mode, a milestone for the implementation of many quantum computing schemes.

A low density layer of InAs self-assembled QDs is grown by molecular beam epitaxy and located at the center of a λ-GaAs microcavity surrounded by two $Al_{0.1}Ga_{0.9}As/Al_{0.95}Ga_{0.05}As$ Bragg mirrors with 20(24) pairs. The quality factor of the planar microcavity is $Q = 4500$. The planar cavity is spin coated with a positive photoresist and inserted in a helium flow cryostat mounted on a motorized positioning system with piezoelectric actuators, providing a 20 nm accuracy. Two laser beams are focused onto the same area of the sample with a microscope objective. A red laser beam ($750\,\text{nm} < \lambda < 830\,\text{nm}$) is used to measure the QD emission, without affecting the photoresist, while a green laser beam ($\lambda = 532$ nm) is used to expose the photoresist (Fig. 1). The focusing of the two beams and their superposition is checked using a monitor camera with a 200× magnification.

The red excitation gives rise to a photoluminescence (PL) emission which is spectrally analyzed using a spectrometer and a charge coupled device camera. The QDs emission is filtered by the planar cavity mode which energy $E_c(\theta)$ blueshifts with the collection angle θ [24]. As a result, QD emission within a 15 meV spectral range can be observed, corresponding to the 0.5 numerical aperture of our microscope objective. The typical PL spectrum in Fig. 1(c). shows a background emission between 1.344 and 1.359 eV corresponding to an emission in the cavity mode for collection angles between $\theta = 0°$ and $\theta_{\text{max}} = 30°$. The single QD exciton (X) emission appears as discrete lines.

 © 2008 The American Physical Society

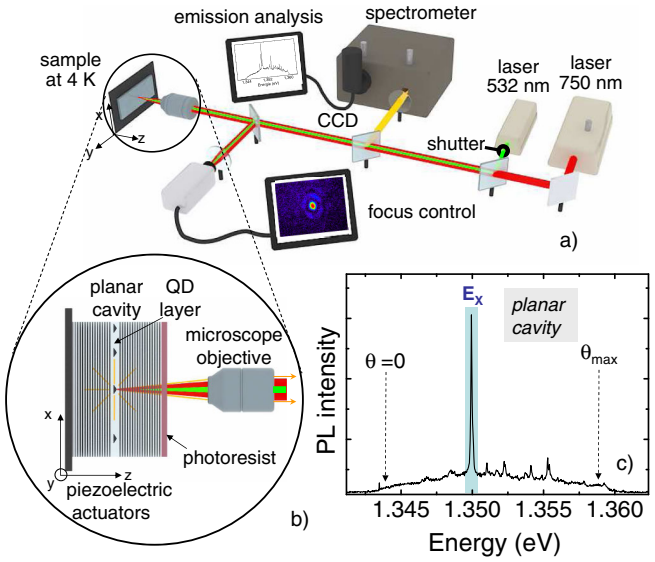

FIG. 1 (color online). (a) Schematic diagram of the experimental setup. (b) Schematic illustrating the method. (c) PL spectrum measured on the planar cavity during the photolithography process.

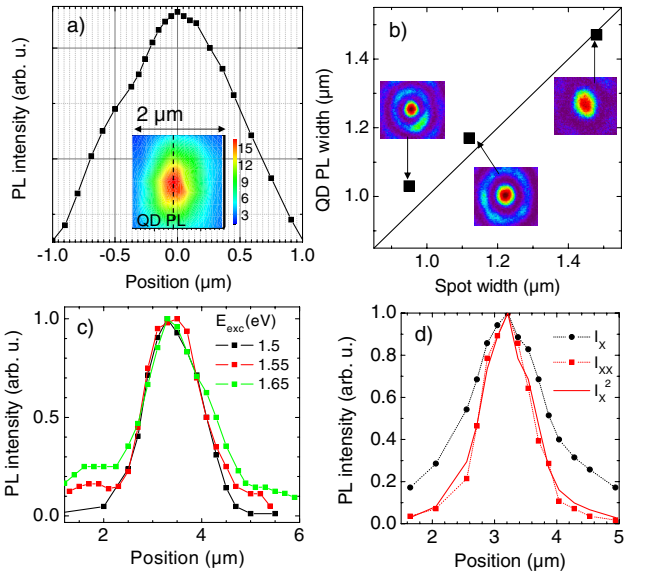

FIG. 2 (color online). (a) QD PL intensity as a function of the sample position, along the dotted line on the inset image. Inset: Mapping of the QD exciton emission intensity as a function of the sample position. (b) QD PL spatial dependence width as a function of the excitation spot width on the sample. The insets show 6.4 μm $\times$ 6 μm images of the excitation laser spot on the control camera. (c) QD PL intensity as a function of the sample position for various E_{exc}. (d) red or gray square (respectively, black circle): Normalized PL intensity of the X (respectively, XX). Red or gray line: square of the X PL intensity.

By scanning the sample position in a few micrometer range, a QD is selected. The sample position is then scanned with respect to the excitation spot with a 20 nm accuracy. The inset in Fig. 2(a). shows a mapping of the selected X emission intensity as a function of the sample position, measured below the X saturation [25]. Figure 2(a) shows an intensity profile of the mapping along the dotted line indicated in the inset. The QD X emission presents a Gaussian-like intensity dependence with a width around 1 μm, reflecting the laser Gaussian profile. The same measurement is performed for various focusing. Figure 2(b) shows that the QD PL intensity width is directly given by the size of the excitation spot. This observation indicates that the capture into the QD is highly efficient and diffusion outside the excitation spot negligible. Indeed Fig. 2(c) shows that the Gaussian dependence is unchanged for excitation energy E_{exc} between 1.5 and 1.6 eV and only slightly broadens for 1.65 eV. Scattering outside the excitation spot only manifests itself by a stronger signal outside the excitation spot.

Mapping the QD signal allows us to determine the QD position by pointing the maximum of the QD X emission, as shown in Fig. 2(a). With a zero noise-to-signal ratio, we would get an accuracy limited by the QD lateral size. With the noise-to-signal ratio of our setup (0.4%), moving the QD within 50 nm from the center of the excitation spot results in no measurable change in the QD signal. As a result, the QD position is pointed with a $\pm$50 nm accuracy. This accuracy could be further improved by using sharper excitation beam profile or by monitoring a nonlinear optical transition of the QD as shown in Fig. 2(d). The biexciton (XX) spatial dependence [red (or gray) scatter line], is given by the square of the exciton spatial dependence [red (or gray) line] [26].

When a QD of desired energy is selected and its emission intensity maximized to position the QD at the very center of the red spot, the green laser is switched on to expose the resist. The exposed area will later be used directly to define the pillar microcavity. This first step ensures the positioning of the QD at the maximum of the pillar fundamental mode.

To reach the spectral matching, one needs to adjust the pillar radius R. As shown in Fig. 3(a), the energy of the pillar fundamental mode increases as the radius decreases [27]. For the example presented in Fig. 1(c), the energy of the selected QD exciton is $E_X = 1.350$ eV and would be resonant to the fundamental mode of a pillar with $R =$ 1 μm. The key to achieve spectral matching is to expose the resist for a well chosen time. Indeed, the chemical change in the resist depends on the exposure dose in a nonlinear way. Since we use a Gaussian laser beam, the size of the exposed area increases with exposure time or laser power. The radius of the developed resist area is presented on Fig. 3(b) as a function of the exposure time for a fixed laser power. Radii ranging from below 0.5 μm to 1.5 μm are reached. Thus, to match the QD selected in Fig. 1(c), the sample is exposed for 30 s in order to obtain a 1 μm radius pillar. After exposing the resist for several QDs, the photoresist is developed, leaving circular holes centered on the selected QDs. After a lift-off step, these holes define the mask to fabricate the pillar through chloride reactive ion etching. A scanning electron microscopy

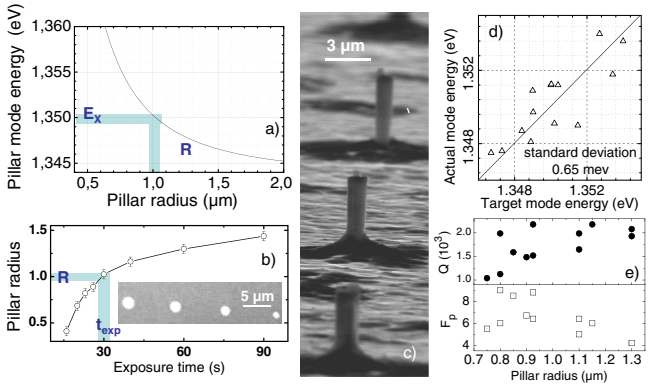

FIG. 3 (color online). (a) Energy of the pillar fundamental mode as a function of the pillar radius. (b) Pillar radius as a function of the resist exposure time for a 532 nm laser power of 500 μW. Inset: Image of the Ni mask obtained after the lift-off of the resist. (c) Scanning electron microscope image of pillars with various radii designed to match QDs with various emission energies. (d) Actual mode energy as a function of target mode energy. (e) Quality factor and Purcell factor as a function of the pillar radius.

image of pillars of various radii designed to match QDs of various energies is presented in Figs. 3(c) and 3(d) shows the obtained mode energy as a function of the target mode energy. A standard deviation as small as 0.65 meV is achieved limited by the verticality of the pillar sidewall and the accuracy of the green laser focus. Finally, Fig. 3(e) presents the quality factor Q of the pillars and their Purcell factor F_p. A mean F_p of 6.4 is achieved. The standard deviation of 1.4 is mainly caused by oscillations of Q predicted in [28]. Yet, obtaining homogeneous F_p is not critical to achieve large scale integration of efficient single photon sources: the extraction efficiency $F_p/(F_p + 1)$ is close to 1 for $F_p \gg 1$.

To prove the high quality of the cavity-exciton spatial matching, optical measurements are performed on the pillars. The PL spectrum of a selected QD is shown in Fig. 4(a) during the lithography step (bottom). For this QD, the exposure time was chosen to obtain a pillar with $R = 0.85$ μm (pillar 1), to match the exciton energy of 1.35 eV. The middle and upper parts of Fig. 4(a) present the PL spectra measured at 10 and 32 K after etching. At 10 K, the X emission is greatly enhanced and the fundamental optical mode (M) of the pillar appears as a base to the X line. Spectral matching is reached at 10 K, as intended. When increasing temperature up to 32 K, the two lines become detuned [14] and well resolved. To get a better insight, PL spectra were acquired over a continuous range of temperatures from 18 to 32 K [Fig. 4(b)]. A strong increase of the QD emission is observed at resonance with the optical mode, showing the acceleration of the radiative lifetime for the X [23]. The linewidth of the optical mode out of resonance is $\gamma_c = 0.89$ meV ($Q = 1500$) so that the expected Purcell factor for a QD perfectly matched to the optical mode is 8.5 [29]. To estimate the actual F_P experienced by the QD, we follow the method presented in [30]. The maximum X PL signal at saturation is measured as a function of the X—cavity detuning Δ [Fig. 4(c)]. This maximum intensity is proportional to $p_X^{\mathrm{sat}}(\Delta)F_{P,\Delta}$, where $p_X^{\mathrm{sat}}(\Delta)$ is the occupation probability of the QD exciton at saturation and $F_{P,\Delta}$ is the Purcell factor depending on detuning [30]. F_P is the maximum Purcell factor for the QD at exact spatial and spectral resonance with the optical mode. We take $F_{P,\Delta} = F_P/(1 + 4\frac{\Delta}{\gamma_c}2)$ and $p_X^{\mathrm{sat}}(\Delta) = 1/(\sqrt{2 + 2F_{P,\Delta}})$ assuming that the XX decay rate is half

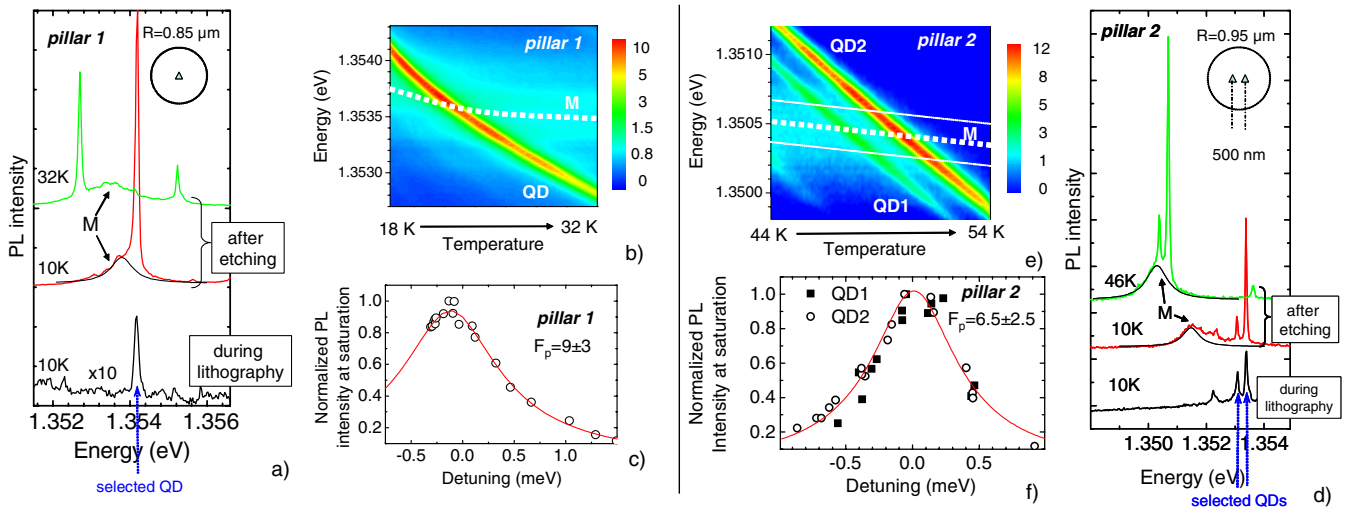

FIG. 4 (color online). (a) [respectively, (d)]: Bottom: PL spectrum measured during the photolithography process at 10 K. Middle and top: PL spectra of pillar 1 (respectively, pillar 2) after etching at 10 and 32 K (respectively, 46 K) (a Lorentzian fit to the mode M is also shown). (b) [respectively, (e)] PL spectra between 18 and 32 K [respectively, 44 and 54 K] measured on pillar 1 (respectively, pillar 2). (c) Pillar 1: Circles: PL intensity of the X line measured at saturation as a function of detuning with the optical mode: $\Delta = E_M - E_X$. Line: fit to the data with $F_P = 9 \pm 3$. (f) Pillar 2: Squares (circles): PL intensity measured at saturation of the QD1 (QD2) X line as a function of detuning with the optical mode: $\Delta_{1(2)} = E_M - E_{\mathrm{QD1(2)}}$. Line: fit to the data with $F_P = 6.5 \pm 2.5$ for both QDs.

the X one. The best fit to the experimental data gives $F_P = 9 \pm 3$, close to the expected value, showing the high quality of the QD spatial matching to the optical mode. Indeed, considering an accuracy of 50 nm for the spatial positioning of the QD, we calculate that the QD is at least at 98% of the maximum of the mode intensity. This value remains as large as 94% for a 0.5 μm radius pillar.

We now demonstrate that our technique can be used to couple two QDs to the same optical mode in a deterministic way. During the lithography step, two QDs can be found to be close to each other both spectrally and spatially. As in the case of a single QD, our method can be used to define a resonant pillar embedding both QDs: as the QD positions are identified, the resist is exposed with the laser spot centered halfway between both QDs. This is what has been implemented for two QDs found to be located 500 nm apart and presenting exciton resonances separated by 300 μeV [Fig. 4(d)]. Both QDs were inserted in a $R = 0.95$ μm radius pillar (pillar 2). After etching, the emission of both QDs is slightly detuned from the pillar mode at 10 K. At 46 K, when bringing the two Xs close to resonance with the optical mode, an increase of both X emissions is observed (top spectrum). Figure 4(e) displays the temperature dependence of the emission spectra measured between 45 and 57 K which highlight the crossing of both lines with the optical mode. For both QDs, a strong increase of the signal is observed at resonance (47 K for QD1 and 49 K for QD2), showing that both Xs experience a Purcell effect. Figure 4(f) shows the normalized signal at saturation for both QDs, as a function of their detuning with the optical mode [31]. Both QDs present the same signal variation as a function of detuning, proving that we have succeeded in equally coupling two QDs to the same optical mode. The fit to the data gives $F_P = 6.5 \pm 2.5$ for both QDs. The quality factor of this pillar is $Q = 2350$ ($\gamma_c = 0.57$ meV) so that the maximum F_p is supposed to be 9. Since the QDs have been located 250 nm away from the center of the pillar, their overlap to the fundamental mode is reduced to 82%, so that the expected F_p is 7.3, very close to the measured value.

In conclusion, we have shown that *in situ* far-field optical lithography can be used to achieve both the spatial and spectral matching of a single QD with a pillar microcavity. A dozen devices have been fabricated on the same sample, within a single lithography step. Each device evidences a strong Purcell effect, showing the scalability of the technique. For the present sample, we intentionally decided to match the quantum dot of various energies to show the flexibility of the spectral tuning. To go toward large scale integration of efficient single photon sources, the present technique could be automatically operated to select QDs within a narrow spectral range and fabricate arrays of cavity-QD devices at the desired wavelength. Processing higher quality factor planar cavities [32] will straightforwardly lead to scalable deterministic strong coupling regime. This technique could also be used to register many kinds of nanostructures in an easy, flexible, and scalable way.

This work is partially supported by the ANR MICADOS and the SANDIE European Network. The authors thank P. Voisin and K. Karrai for fruitful discussions.

*Also at Université Paris Diderot, 10 rue Alice Domon et Léonie Duquet, 75205 Paris, France.
†pascale.senellart@lpn.cnrs.fr

[1] For a review, see *Handbook of Self Assembled Semiconductor Nanostructures for Novel Devices in Photonics and Electronics*, edited by M. Henini (Elsevier, New York, 2008).
[2] A. Peter Lodahl *et al.*, Nature (London) **430**, 654 (2004).
[3] B. Lounis and W. E. Moerner, Nature (London) **407**, 491 (2000).
[4] P. Michler *et al.*, Science **290**, 2282 (2000).
[5] M. Pelton *et al.*, Phys. Rev. Lett. **89**, 233602 (2002).
[6] E. Moreau *et al.*, Appl. Phys. Lett. **79**, 2865 (2001).
[7] E. M. Purcell, H. C. Torrey, and R. V. Pound, Phys. Rev. **69**, 37 (1946).
[8] A. Imamoglu *et al.*, Phys. Rev. Lett. **83**, 4204 (1999).
[9] M. Feng, I. D'Amico, P. Zanardi, and F. Rossi, Phys. Rev. A **67**, 014306 (2003).
[10] M. N. Leuenberger, Phys. Rev. B **73**, 075312 (2006).
[11] F. Meier and D. D. Awschalom, Phys. Rev. B **70**, 205329 (2004).
[12] T. Yoshie *et al.*, Nature (London) **432**, 200 (2004).
[13] J. P. Reithmaier *et al.*, Nature (London) **432**, 197 (2004).
[14] E. Peter *et al.*, Phys. Rev. Lett. **95**, 067401 (2005).
[15] N. LeThomas *et al.*, Nano Lett. **6**, 557 (2006).
[16] Y.-S. Park, A. K. Cook, and H. Wang, Nano Lett. **6**, 2075 (2006).
[17] A. Hartmann *et al.*, Appl. Phys. Lett. **71**, 1314 (1997).
[18] S. Kiravittaya *et al.*, Appl. Phys. Lett. **89**, 233102 (2006).
[19] Z. G. Xie and G. S. Solomon, Appl. Phys. Lett. **87**, 093106 (2005).
[20] A. Rastelli *et al.*, Appl. Phys. Lett. **90**, 073120 (2007).
[21] K. Hennessy *et al.*, Appl. Phys. Lett. **87**, 021108 (2005).
[22] H. Lohmeyer *et al.*, Appl. Phys. Lett. **92**, 011116 (2008).
[23] A. Badolato *et al.*, Science **308**, 1158 (2005).
[24] A. Arena *et al.*, Appl. Phys. Lett. **72**, 2571 (1998).
[25] K. Brunner, G. Abstreiter, G. Böhm, G. Tränkle, and G. Weimann, Phys. Rev. Lett. **73**, 1138 (1994).
[26] P. Senellart *et al.*, Phys. Rev. B **72**, 115302 (2005).
[27] J. M. Gérard *et al.*, Appl. Phys. Lett. **69**, 449 (1996).
[28] Ph. Lalanne, J. P. Hugonin, and J. M. Gérard, Appl. Phys. Lett. **84**, 4726 (2004).
[29] J. M. Gérard *et al.*, Phys. Rev. Lett. **81**, 1110 (1998).
[30] C. Böckler *et al.*, Appl. Phys. Lett. **92**, 091107 (2008).
[31] Surprisingly, the PL intensity of the two QDs is different whereas it was quite similar during the lithography step. The same effect is observed on another pillar embedding two QDs This effect is currently under investigation.
[32] S. Reitzenstein *et al.*, Appl. Phys. Lett. **90**, 251109 (2007).